

Processing and Characterization of Graphene and Multi-wall Carbon Nanotube-Reinforced Aluminium Alloy AA2219 Composites Processed by Ball Milling and Vacuum Hot Pressing

Lava Kumar Pillari¹ · A. K. Shukla² · S. V. S. Narayana Murty² · V. Umasankar¹

Received: 9 February 2017/Revised: 11 May 2017/Accepted: 8 June 2017/Published online: 23 June 2017
© Springer Science+Business Media, LLC and ASM International 2017

Abstract Aluminium alloy AA2219 reinforced with graphene/MWCNT nanocomposites having near theoretical densities has been successfully fabricated by high-energy ball milling followed by vacuum hot pressing. Effect of varying graphene and MWCNT content was studied on different aspects of processing of the composites. The particle size increases during milling due to cold welding; but the presence of reinforcement restricts and the resultant microstructures exhibited a layered morphology with graphene/MWCNT between particle boundaries. The composite with 0.5 wt.% reinforcement (graphene/MWCNT) content exhibited peak hardness, and further additions led to a decrease in hardness owing to the agglomeration of reinforcement at particle interfaces. The present study reveals that graphene is a better reinforcement compared to MWCNTs in aluminium matrix. This is attributed to the sheet-like morphology of graphene which covers the matrix powder particles more effectively compared to tube-like MWCNTs in providing more matrix–reinforcement contact points leading to better sintering.

Keywords AA2219 alloy · Graphene · MWCNT · Ball milling · Vacuum hot pressing

Introduction

The quest for materials with higher strength and stiffness led to the development of composite materials. In composites, the strength and stiffness are tailored by incorporating suitable reinforcements in the matrix. The matrix under load transfers and distributes it to the reinforcement. The area of metal matrix composites (MMCs) is an important field of advanced materials attracting many researchers due to their superior properties, such as higher stiffness, higher strength-to-weight ratio, low thermal expansion coefficient and high wear resistance compared to monolithic materials. Such characteristics make MMCs suitable for engineering applications in automobile, aviation, defence and marine industries [1–5]. Lighter materials like magnesium, aluminium, copper, titanium and its alloys are normally used as matrix materials for MMCs. Among these matrices, aluminium and its alloys are most sought as a matrix material in the development of metal matrix composites due to their light weight, high specific strength, good thermal and electrical conductivity [2, 4, 6, 7]. Researchers fabricated aluminium matrix composites with various reinforcements such as SiC [8, 9], graphite [10], TiC [11], Al₂O₃ and B₄C [12].

Recently, aluminium reinforced with nanosize reinforcements attracted many researchers in view of their unique mechanical, thermal, electronic and biological properties, which are not possible with their conventional micron-sized counterparts. Carbonaceous materials like graphene and carbon nanotubes (CNTs) are the most researched nanomaterials as reinforcements in aluminium matrix composites [13, 14]. Graphene is the basic building block for all the carbonaceous materials like fullerenes (0-dimensional), CNTs (2-dimensional) and graphite (3-dimensional) [15] and was experimentally

✉ S. V. S. Narayana Murty
susarla.murty@gmail.com;
narayanamurty_susarla@vssc.gov.in

¹ School of Mechanical and Building Sciences, VIT University, Vandalur-Kelambakkam Road, Chennai 600127, India

² Materials and Metallurgy Group, Vikram Sarabhai Space Centre, Trivandrum 695022, India

demonstrated to be a good reinforcement [16]. Graphene is a flat sheet of single-layered sp²-bonded carbon atoms tightly packed into a benzene ring structure [17, 18]. Graphene possesses excellent modulus of elasticity (1 TPa) [19], thermal conductivity (5000 W/mK) [20], charge carrier mobility (2×10^5 cm²/Vs) [21], surface area (2600 m²/g) [22] and intrinsic strength (130 GPa) [19]. Carbon nanotubes (CNTs) were graphene sheets rolled up in the shape of nanometre-sized cylinders [23]. Single-walled and multi-walled CNTs are formed by roll-up of single and multi-layers of graphene sheets, respectively [14, 16]. CNTs show excellent properties, Young's modulus of 1 TPa [24], tensile strength in the region of 150 GPa [25] and surface area in the range of 150–1500 m²/g [26]. All these properties make graphene and CNTs ideal as strengthening additives for aluminium matrix composites. However, the dispersion of graphene/CNTs into an aluminium matrix and good interfacial bonding between the reinforcement and matrix are the main challenges restricting the development of these composites.

To reduce the agglomeration/clustering of CNTs/graphene, many researchers used ball milling (mechanical alloying) to disperse graphene/CNTs in aluminium matrix [5, 27–30]. Liu et al. [31] investigated the effect of ball milling time on aluminium-CNT composites and observed a uniform dispersion of CNTs in aluminium matrix after 6 h ball milling. In another study, Esawi and Morsi [32] investigated the effect of ball milling time on Al-CNT composite powders, and it was reported that the individual CNTs are embedded in aluminium matrix after 48 h of ball milling. Hot pressing of milled powders is a very effective means of obtaining compacts with near theoretical density. However, there are only few reports on fabrication of aluminium-graphene/CNT composites using mechanical alloying followed by hot pressing. Tables 1 and 2 show the processing techniques and resultant properties of aluminium-graphene and aluminium-CNT composites, respectively. Even though several researchers have studied these composites, their effectiveness as reinforcement has not been addressed.

Therefore, the objective of the present study is to develop an aluminium alloy AA2219-graphene/MWCNT composites using high-energy ball milling followed by vacuum hot pressing under identical conditions. The ball-milled powders are characterized by x-ray diffraction (XRD), scanning electron microscopy (SEM) and differential scanning calorimetry (DSC) and the hot-pressed samples characterized by using optical microscopy, SEM, Raman spectroscopy and hardness testing to study the effectiveness of each of the reinforcements in aluminium alloy matrix.

Materials and Experimental Details

Materials Characteristics

Aluminium alloy AA2219 powder (average particle size: 38 μm) was employed as the matrix material. Chemical composition of as-received aluminium alloy AA2219 powder is given in Table 3. Multi-walled carbon nanotubes (MWCNT) (diameter: ~Ø 20 nm, length: 50 μm, purity >97%) and graphene (diameter: ~Ø 0.5–1 μm, thickness: 0.8–1.6 nm, purity >95%) were used as reinforcements. The SEM images presented in Fig. 1 show the morphologies of the graphene and MWCNT used in this study.

Methods

Graphene/MWCNTs were dispersed in AA2219 matrix by mechanical alloying of AA2219 with 0, 0.5, 1 and 2 wt.% of MWCNT/graphene using high-energy ball milling. The milled composite powders were sintered by vacuum hot pressing.

High-Energy Ball Milling

AA2219-graphene and AA2219-MWCNT composite powders were prepared by high-energy ball milling using planetary ball mill. Compositions were prepared by varying the graphene and MWCNT percentage (0, 0.5, 1 and 2 wt.%). Measured amounts of MWCNTs and graphene were mixed separately with aluminium alloy AA2219 powder in a stainless steel jar containing balls of 10 mm diameter giving the ball-to-powder ratio (BPR) of 4:1. Ball milling was carried out at a rotating speed of 200 rpm for 6 h. To study the effect of ball milling alone, as-received aluminium alloy AA2219 powder was also ball-milled for 6 h without any reinforcement. Toluene was used as the process controlling agent (PCA) during the ball milling to minimize cold welding and to prevent powder sticking on the milling media and walls of the stainless steel container.

Vacuum Hot Pressing (VHP)

Vacuum hot pressing was carried out in a graphite die with using 100 MPa uniaxial load in a 250 T capacity/2000 °C rated industrial vacuum hot press. Figure 2 shows the temperature cycle used during the processing of composites by vacuum hot pressing. A sintering temperature of 500 °C, holding time of 30 min and a heating rate of 10 °C/min were used during hot pressing. Constant load of 100 MPa was applied for the entire hot pressing cycle until the initiation of the cooling cycle. Table 4 shows the composition of samples and their nomenclature.

Table 1 Summary of the various powder metallurgy-based techniques and resultant properties of Al + graphene composites

Composite	Processing techniques	Properties	References
Al + 0.1 wt.% graphene	Ball milling HIP: 375 °C, 20 min	Vickers hardness: 99 HV Yield strength: 198 MPa	Bartolucci et al. [33]
Al + 0.15 wt.% GNSs	Sonication followed by stirring Cold compaction: 560 MPa Tube furnace: 600 °C, 5 °C/min, 240 min	Vickers hardness: 37.6 HV	Liu et al. [34]
Al + 0.3 wt.% graphene	Ball milling: 325 rpm Sintering: 580 °C, 120 min Hot extrusion: 440 °C, 20:1	Tensile strength: 249 MPa	Wang et al. [17]
Al + 0.3 wt.% graphene	Ultra-sonication: 60 min Ball milling: 60 min Cold compaction: 170 MPa Sintering: 600 °C, 360 min Hot extrusion: 470 °C, 1 m/min	Vickers hardness: 85 HV Yield strength: 195 MPa UTS: 280 MPa	Rashad et al. [18]
Al + 0.3 wt.% graphene	Ultra-sonication followed by stirring Powder metallurgy: 600 °C, 25 MPa, 60 min	UTS: 110 MPa	Gao et al. [35]
Al + 1 wt.% graphene	Ball milling: 5:1, 120 min Cold compaction: 950 MPa, Sintering: 500 °C, 120 min, 5 °C/min	Vickers microhardness: 93 HV	Bustamante et al. [36]
Al + 1 wt.% GNP	Blending Cold compaction: 565 MPa Sintering: tubular furnace, 550 °C, 120 min	Vickers microhardness: 46 HV	Alam and Kumar [37]
Al + 1 wt.% GNFs	Cryo milling: 40:1, 180, 120 min Hot extrusion: 300 °C, 17.6:1 Heat treatment: 300 °C, 120 min	Yield strength: 194 MPa UTS: 248 MPa	Li et al. [38]
Al5083 + 1 wt.%, GNP	Ball milling: 20:1, 350 rpm, 24 h Hot pressing: 500 °C, 300 MPa, 1 h Hot extrusion: 500 °C, 1 mm/min, 10:1	Yield strength: 332 MPa UTS: 470 MPa	Zhang et al. [39]
AlMg5 + 1 vol.% GO	Ball milling: 10:1, 20 h Hot pressing: 550 °C, 570 MPa, 4 s	Vickers hardness: 66 HV	Kwon et al. [40]
Al6061 + 1 wt.% graphene	Stirring: 1440 min Ball milling: 60 min HP: 100 MPa, 10 min, 630 °C	Flexural strength: 800 MPa	Bastwros et al. [5]

UTS ultimate tensile strength; HIP hot isostatic pressing; HP hot pressing; GNP graphite nanoplatelets; GNF graphene nanoflakes; GO graphene oxide

Characterization

Powders

The morphology of the ball-milled aluminium alloy AA2219-graphene/MWCNT powders was investigated by using scanning electron microscopy. The average particle size of powder samples was analysed by laser particle size analyser. DSC experiments were carried out for the as-received and milled powders at a constant heating rate of 20 K/min, and subsequently, x-ray diffraction was performed to confirm formation of any reaction phases.

Sintered Compacts

The sinter density of samples was measured by using water displacement method by employing Archimedes principle. Theoretical density (ρ_e) of samples was determined using rule of mixture. The theoretical density of aluminium alloy AA2219, graphene and MWCNT is 2.8, 2 and 2.6 g/cm³, respectively. The relative density of samples was further calculated by dividing experimental density (ρ_e) with theoretical density (ρ_t). The sintered samples were characterized by using optical microscope and Raman spectroscopy. The hot-pressed samples were cut, and

Table 2 Summary of the various powder metallurgy-based techniques and resultant properties of Al + MWCNT composites

Composite	Processing techniques	Properties	References
Al + 0.5 wt.% CNT	Ultra-sonication, can rolling SPS: 500 °C, 20 min Hot extrusion: 500 °C, 9:1, 5 mm/s	Yield strength: 96 MPa UTS: 174 MPa Vickers hardness: 50 HV	Liao et al. [41]
Al + 0.75 wt.% MWCNT	Sonication: 5 min Ball milling: 5:1, 120 min Compaction: 950 MPa Sintering: 550 °C, 180 min	Yield strength: 23 kg/mm ² Vickers hardness: 77 HV	Bustamante et al. [42]
Al + 1 wt.% CNT	Ultra-sonication hot pressing: 50 MPa, 600 °C, 10 °C/min, 30 min SPS: 50 MPa, 600 °C, 50 °C/min, 10 min	Vickers hardness: 49 HV Vickers hardness: 54 HV	Kim et al. [43]
Al + 2.5 wt.% MWCNT	Ball milling: 90 min, 5:1 SPE: 350 °C (10 min) → 433 °C (16:1, 6.3 mm/s)	Vickers hardness: 99 HV Compressive strength: 415 MPa	Morsi et al. [44]
Al + 5 wt.% MWCNT	Ball milling: 240 min Compaction: 220 MPa Hot extrusion: 500 °C, 60 min	Brinell hardness: 140 BH	Majid et al. [45]
Al + 6 wt.% MWCNT	Ball milling: 10:1, 300 rpm, 1200 min Heating: 350 °C, 60 min Compaction: 570 MPa, 10 s Extrusion: 14:1, 1 mm/s	Vickers macrohardness: 151 HV ₂₀	Bradbury et al. [46]
Al2009 + 1 wt.% CNT	Cryogenic milling: 39:1, 180 rpm, 120 min; HIP: 465 °C, 18:1, 2 mm/s Solution treatment: 498 °C, 240 min , Quenching followed by natural ageing for 96 h	UTS: 560 MPa Yield strength: 443 MPa Elongation: 10.2%	He et al. [47]
Al2024 + 1 wt.% CNT	Mechanical stirring Ball milling: 60 min CIP: 300 MPa, 5 min Extrusion: 500 °C, 25:1	Vickers hardness: 136 HV Tensile strength: 474 MPa Yield strength: 336 MPa Young's modulus: 88 MPa	Deng et al. [48]
AA2124 + 2 wt.% CNT	Sonication Wet ball milling: 200 rpm, 1 h, 10:1 Spark plasma sintering: 500 °C, 20 min, 35 MPa	Vickers hardness: 121 HV	Saheb [49]
AA6061 + 2 wt.% CNT	Sonication Wet ball milling: 200 rpm, 1 h, 10:1 Spark plasma sintering: 500 °C, 20 min, 35 MPa	Vickers hardness: 68 HV	Saheb [49]

SPS spark plasma sintering; SPE spark plasma extrusion; UTS ultimate tensile strength; CIP cold isostatic pressing, HIP hot isostatic pressing

Table 3 Chemical composition of AA2219 alloy powder

Element	Cu	Si	Mn	Fe	Zn	Ti	Zr	V	Al
Amount (wt.%)	5.56	0.07	0.28	0.08	0.01	0.07	0.18	0.1	Balance

microstructures of the cross-sectional surface of all samples were observed by an optical microscope. Keller's reagent (2.5 ml HNO₃, 1.5 ml HCl, 1.0 ml HF and 95 ml H₂O) was used as an etching agent. Brinell hardness of the composites was measured using ~Ø 2.54-mm-diameter steel ball as indenter with 30 kgf load. Fracture surfaces of the samples were examined by using SEM.

Results and Discussion

Size and Morphological Changes During Ball Milling of AA2219-graphene/MWCNT Powders

Scanning electron microscopy was used to see the morphological changes during the ball milling of AA2219-

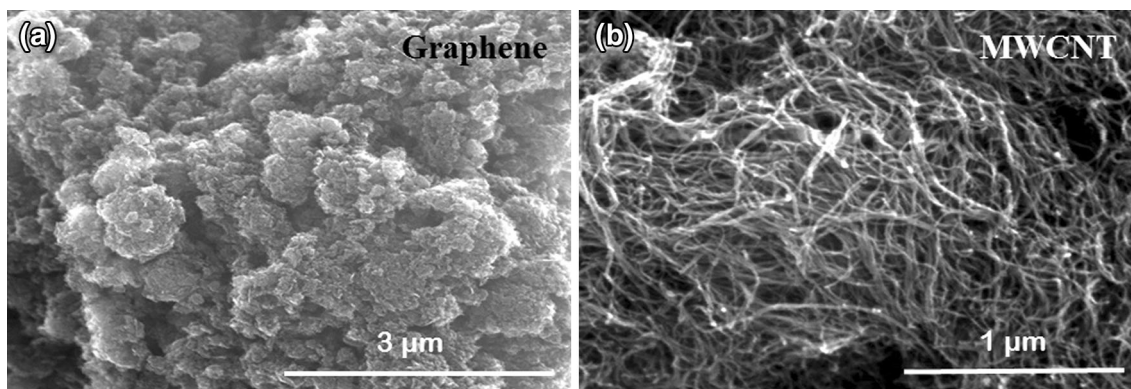


Fig. 1 SEM images showing the morphology of starting materials employed in the present study: (a) the graphene and (b) the MWCNTs

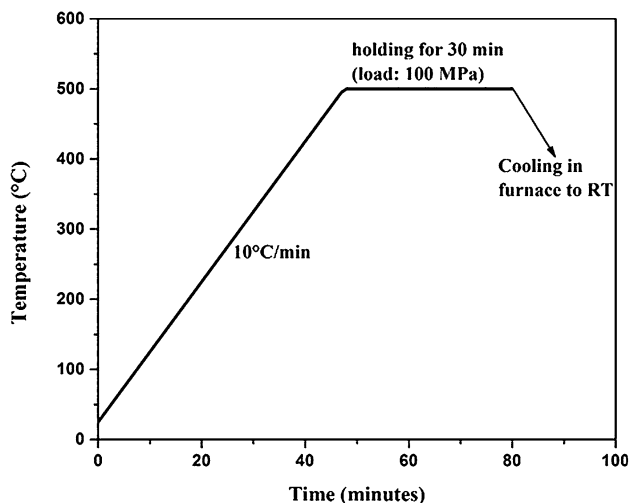


Fig. 2 Temperature cycle used during the processing of composites by vacuum hot pressing

Table 4 Composition of powders used for VHP experiments and their sample identification number

Sl. no.	Composition	Sample ID	
		Powder	VHP
1	AA2219 (as-received)	AR	ARH
2	AA2219 (milled)	AM	AMH
3	AA2219 + 0.5 wt.% graphene	A0.5G	A0.5GH
4	AA2219 + 1 wt.% graphene	A1G	A1GH
5	AA2219 + 2 wt.% graphene	A2G	A2GH
6	AA2219 + 0.5 wt.% MWCNT	A0.5C	A0.5CH
7	AA2219 + 1 wt.% MWCNT	A1C	A1CH
8	AA2219 + 2 wt.% MWCNT	A2C	A2CH

MWCNT/graphene powders, and the figures are shown in Fig. 3a–h. The quantitative information about particle size during ball milling can be obtained from the particle size analysis performed by using laser particle size analyser.

The average particle size of ball-milled AA2219-graphene and AA2219-MWCNT composite powders is presented in Table 5.

Figure 3a shows that the gas-atomized original AA2219 powder has an irregular shape. The powder particles milled for 6 h also exhibit an irregular shape with flattened morphology as shown in Fig. 3b. This may be due to the impact of ball milling media during the milling process [31]. Further, Table 5 shows that the average particle size of AA2219 increased from 38 to 101 μm with 6 h of ball milling. This is due to the cold welding of ductile AA2219 particles. Initially, the AA2219 powder particles deform under the impact of ball milling media forming flake-like shape particles that were eventually cold-welded to form large particles [50, 51]. However, the particle size of samples decreased with addition of reinforcement (graphene/MWCNTs). The particle sizes of 0.5 wt.% graphene/MWCNT sample were 71 and 66 μm, respectively. The particle size further reduced to 68 μm with increase in graphene content to 1 and 2 wt.%. The ductility of the composites decreases with addition of graphene and led to the fracturing of powders. During mechanical alloying (ball milling), cold welding and fracturing mechanisms compete and control the particle size [5, 32, 52]. Contrary to the case of the AA2219-graphene composite powder, different milling behaviour was observed in the case of AA2219-MWCNT composite powders. Here, the particle size increased to 72 and 74 μm with the addition of 1 and 2 wt.% MWCNT, respectively. This may be due to the morphological difference between graphene and MWCNT. Similar observations were reported by Wang et al. [50] and Wu et al. [52]. Compared to sheet morphology of graphene, the tube-like shape of MWCNTs leads to the formation of clusters/agglomerates easily and led to increase in particle size with addition of MWCNT. It was also observed that the size of the AA2219-graphene/MWCNT powder was much smaller than that of the unreinforced AA2219 powders milled under the same condition. It indicates that the

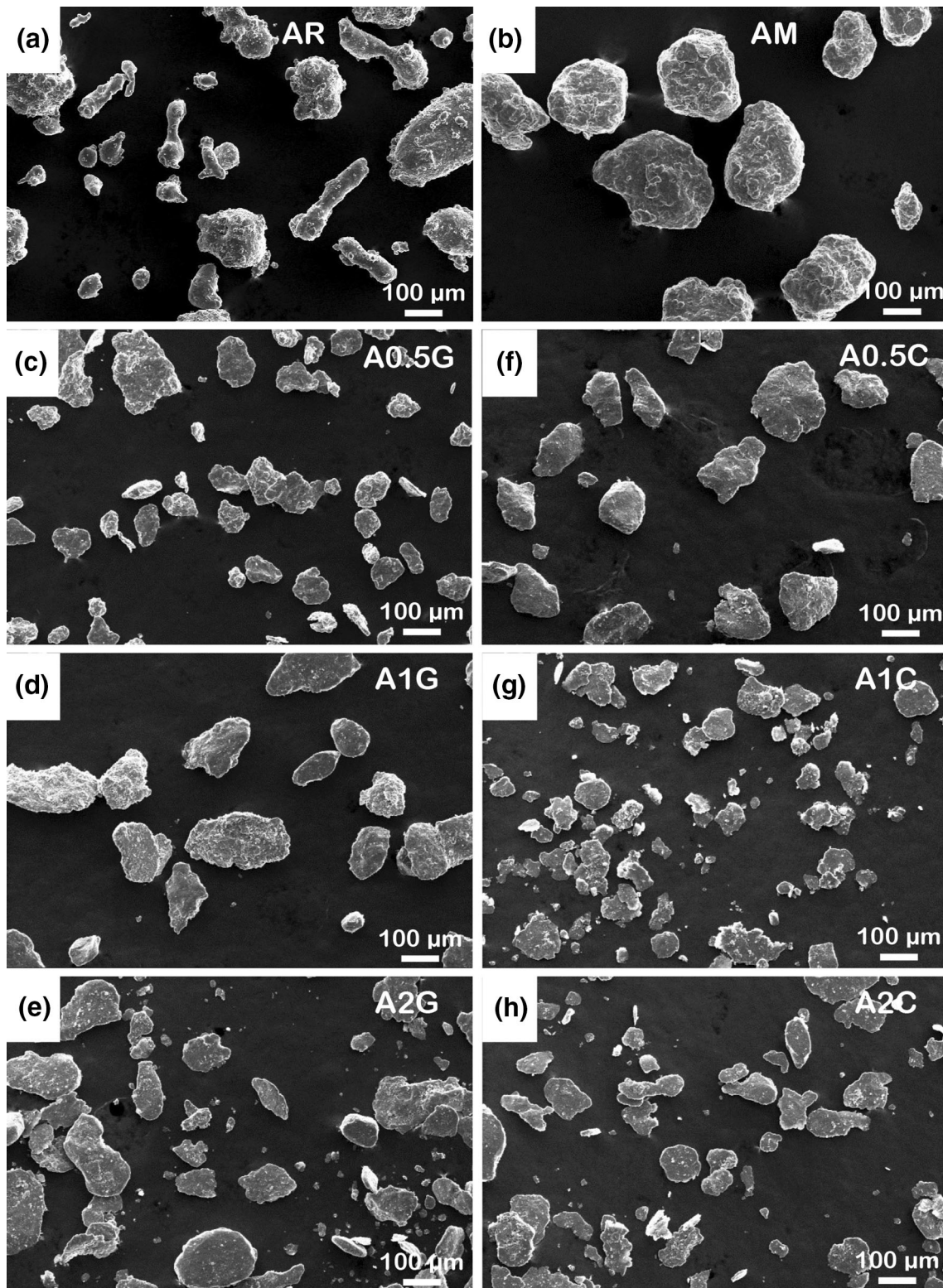


Fig. 3 SEM micrographs showing the morphology of (a) AR, (b) AM, (c) A0.5G, (d) A1G, (e) A2G, (f) A0.5C, (g) A1C and (h) A2C powders

graphene/MWCNTs acted as milling aid, which restricted the growth of particle size during the ball milling [50, 52].

DSC Analysis of Powders

DSC experiments were conducted on the AA2219-graphene (Fig. 4a) and AA2219-MWCNT (Fig. 4b) composite powders to detect possible reactions between matrix and reinforcement. The DSC curves did not show any significant difference between the as-received AA2219 and AA2219-graphene/MWCNT composites. Further, they also did not reveal any phase transformations such as the formation of Al_4C_3 . It indicates that there is no reaction between AA2219 matrix and reinforcement (graphene/MWCNT). However, the DSC curves of both AA2219-graphene and AA2219-MWCNT system show two endothermic peaks at 543 and 660 °C. The endothermic peak at 543 °C can be ascribed to the dissolution of Al_2Cu precipitates in matrix, and the peak at 660 °C can be

ascribed to the melting of aluminium alloy AA2219 [5, 28, 53]. Subsequently x-ray diffraction was performed on the heated samples (residue in the crucible after DSC analysis) to confirm the phases in the DSC-analysed sample.

X-ray Diffraction Analysis

XRD patterns of AA2219-graphene and AA2219-MWCNT are shown in Fig. 5a and b, respectively. All compositions show major aluminium peaks at 38.6°, 44.8°, 65.2°, 78.4°, and 82.6°. The diffraction peaks of Al_2Cu observed in the pattern of original sample before performing DSC analysis (not shown here) are still present. These Al_2Cu precipitates may be formed during the synthesis of aluminium alloy AA2219. This may be attributed to the fact that AA2219 powder synthesized by gas atomization technique is metastable due to supersaturated solution of the alloying elements. Hence, the Al_2Cu precipitates have formed during the cooling. The XRD scans of DSC-analysed samples also show Al_2Cu peaks. During the DSC analysis, the dissolution of Al_2Cu precipitates occurs at 543 °C as shown in Fig. 4 and forms a supersaturated solution of aluminium and copper. Further, the precipitation of Al_2Cu occurs when the powders are cooled slowly after DSC experiment [27, 54]. None of the XRD scans of AA2219-graphene/MWCNT indicated the presence of Al_4C_3 , but this does not rule out the possibility of carbide phase in the material either due to the small volume of carbide, which may be out of the detection limits of XRD or the wt.% of graphene/MWCNT is not sufficient for the reaction to occur [5, 55]. Chunfeng et al. [27] fabricated AA2014 reinforced with 5 wt.% MWCNT composites processed by ball milling

Table 5 Average particle size of as-received and ball-milled AA2219-graphene and AA2219-MWCNT composite powders

S. no.	Sample	Average particle size (µm)
1	AA2219 (as-received)	38
2	AA2219 (6 h milled)	101
3	AA2219 + 0.5 wt.% graphene	71
4	AA2219 + 1 wt.% graphene	68
5	AA2219 + 2 wt.% graphene	68
6	AA2219 + 0.5 wt.% MWCNT	66
7	AA2219 + 1 wt.% MWCNT	72
8	AA2219 + 2 wt.% MWCNT	74

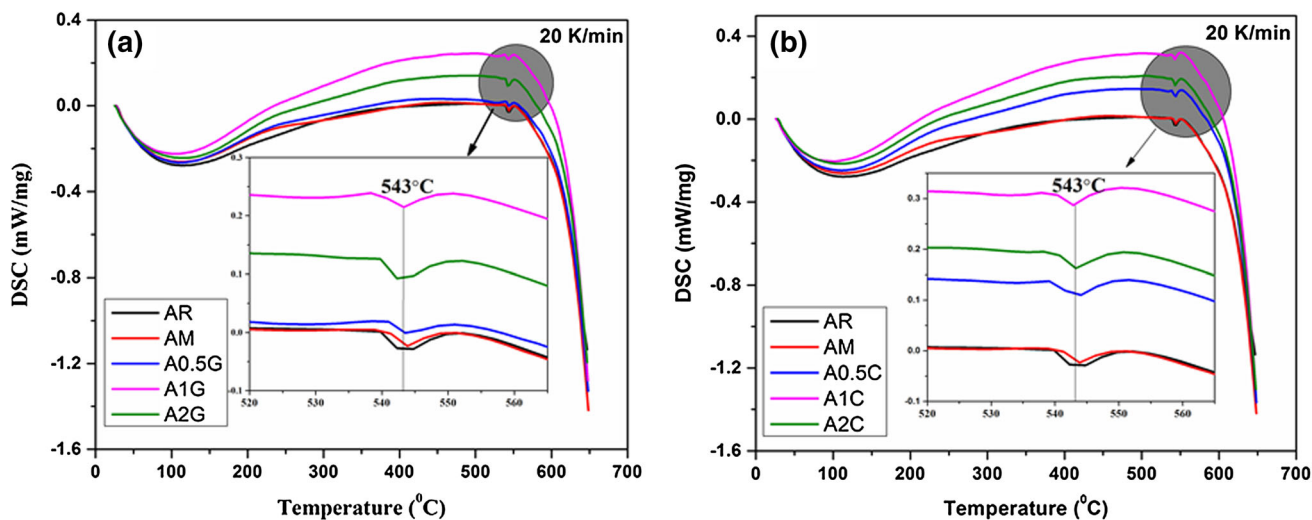


Fig. 4 DSC plots of (a) AA2219 and AA2219—graphene powders, and (b) AA2219 and AA2219—MWCNT powders

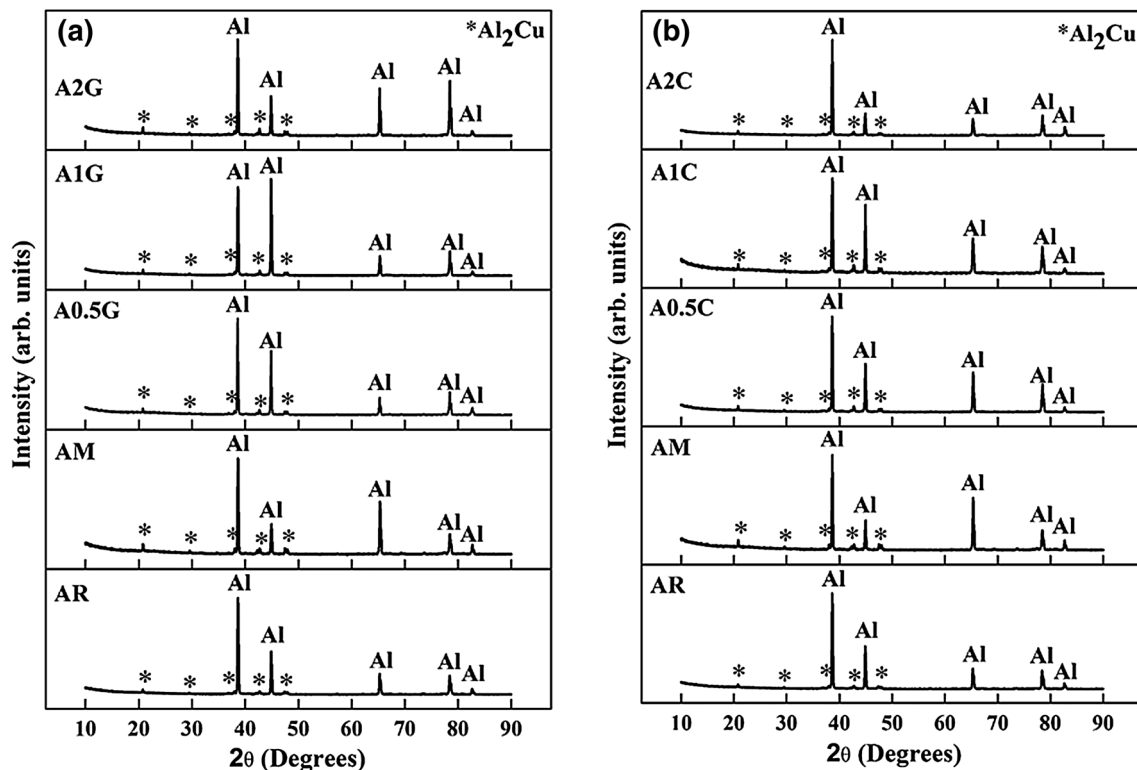


Fig. 5 X-ray diffraction patterns of (a) AA2219 and AA2219-graphene and (b) AA2219 and AA2219-MWCNT composite powders performed after performing DSC analysis at 20 K/min

followed by hot pressing at a temperature of 600 °C and observed the formation of Al_4C_3 . None of the XRD scans of the samples revealed the presence of graphene/MWCNT in AA2219 matrix. A similar observation was reported by other researchers [56]. This may be attributed due to the limitation in XRD detection.

Raman Analysis

As x-ray diffraction did not reveal the presence of graphene/MWCNT in the milled composite powders, Raman analysis was performed to confirm their presence in the aluminium alloy AA2219 matrix. The Raman spectra of AA2219-graphene and AA2219-MWCNT composites are shown in Fig. 6. The spectra show two characteristic peaks of graphene/MWCNT, namely D and G band, appearing at around 1340 and 1590 cm^{-1} , respectively. The D band represents the vibration of carbon atoms with disordered structure (amorphous carbon, dopants, vacancies or defects) in graphene/MWCNTs. The presence of D band in the materials is attributed to the structural defects. The G band is attributed to the vibration of carbon atoms of the graphite [57–60]. Raman analysis confirms the presence of graphene/MWCNT in AA2219 matrix.

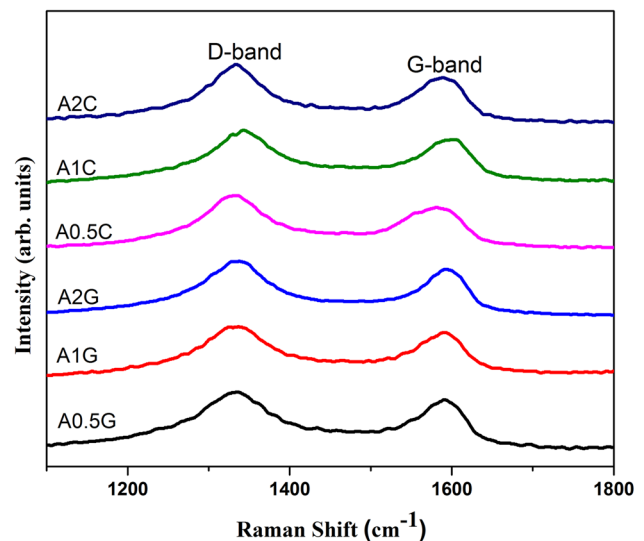


Fig. 6 Raman spectra of the ball-milled AA2219-graphene and AA2219-MWCNT composites

Relative Density

The effect of graphene/MWCNT content on the relative density of samples is shown in Fig. 7a and b, respectively. All the vacuum hot-pressed samples show a relative

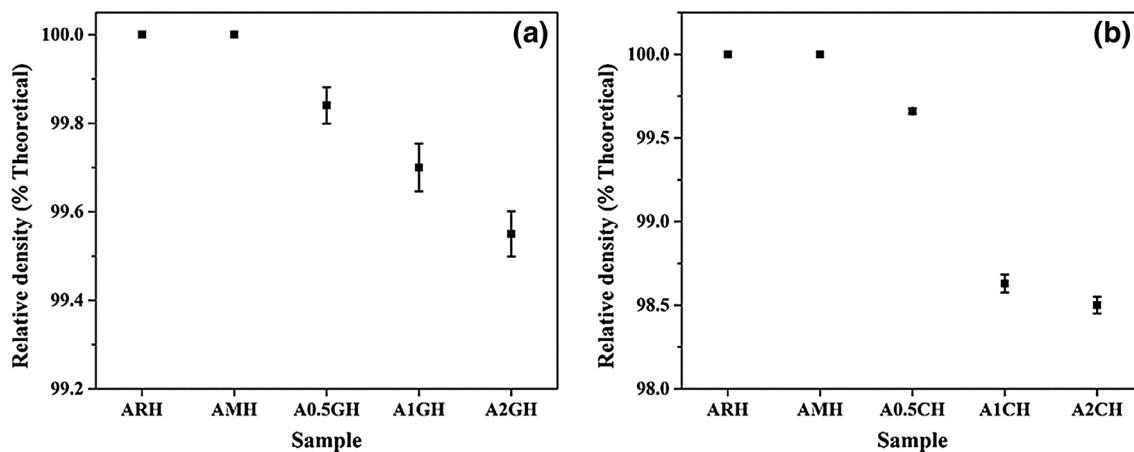


Fig. 7 Relative density of (a) AA2219-graphene and (b) AA2219-MWCNT composites with different reinforcement contents fabricated by vacuum hot pressing

density of more than 98%. However, the relative density decreases with the addition of reinforcement (graphene/MWCNT). At higher reinforcement contents, the densification becomes more difficult because the formation of graphene/MWCNT clusters at interface restricts the particle boundary diffusion [61]. The presence of graphene/MWCNT at particle boundaries is revealed as dark regions in optical microscopy as shown in Fig. 8. Esawi and El Borady [62] also observed a decrease in density with 2 wt.% MWCNT addition.

Microstructural Observations

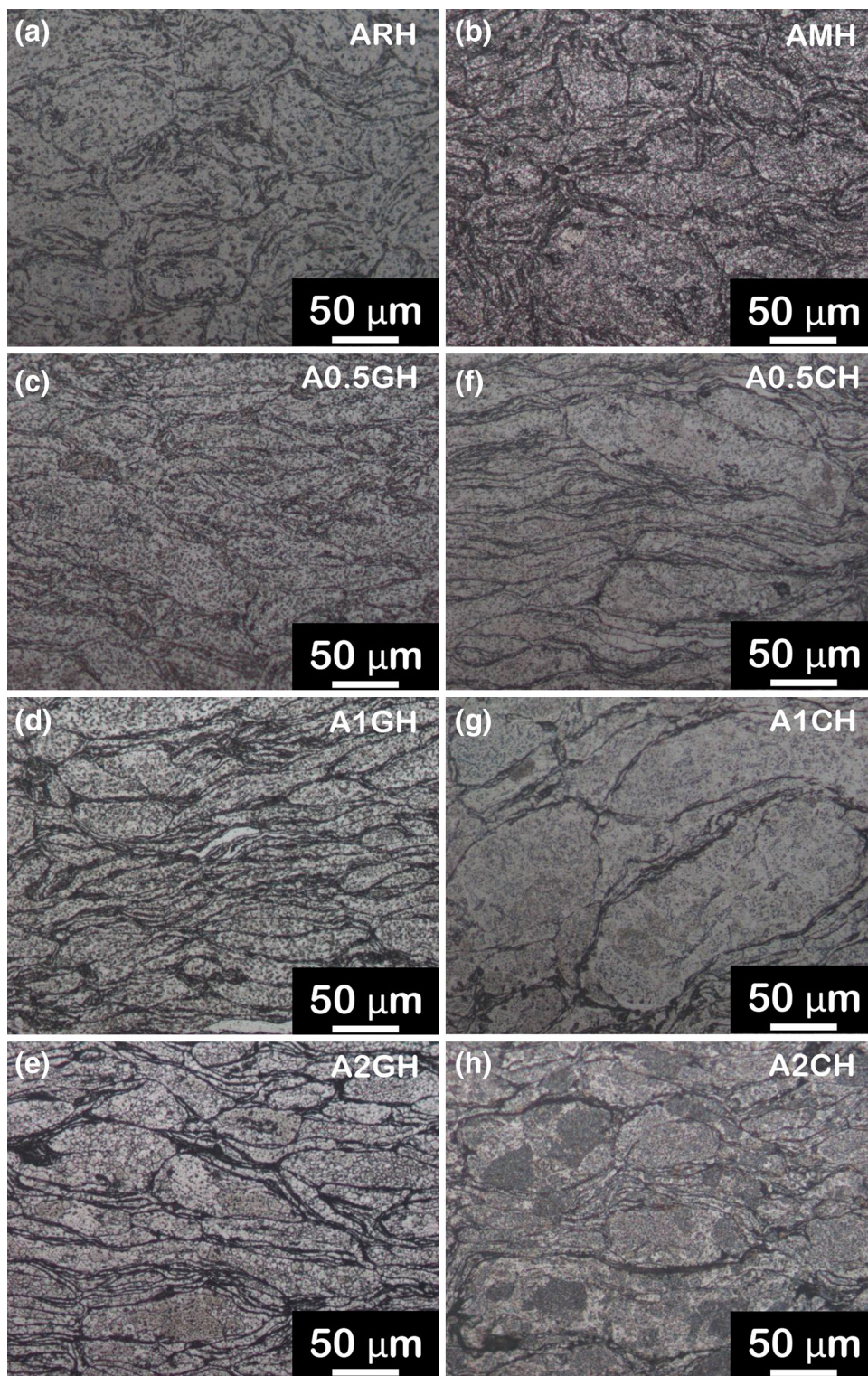
Figure 8a–h shows the optical micrographs of the polished cross sections of the AA2219-graphene/MWCNT composites. Figure 8a–h shows that all the sintered compacts are almost dense. The as-received AA2219 compact has an equiaxed microstructure which is different compared to all other samples (Fig. 8a). However, with 6 h ball milling, the structure changes from an equiaxed to a layered morphology, as shown in Fig. 8b. During the ball milling of AA2219 powder, each particle deforms plastically and forms an individual flake, and with further ball milling the cold welding of individual flakes occurs. During hot pressing, the cold-welded AA2219 flakes bond to each other and form layered morphology. The microstructure of AA2219 reinforced with graphene/MWCNT composites has layered morphology with graphene/MWCNT (dark layer) between the grains. The severity of layered morphology increases with increasing content of graphene/MWCNT, and this is supported by fact that the grains deformed more and more with increasing reinforcement content. This may be attributed to the presence of graphene/MWCNTs along the grain boundaries which makes the grains to deform perpendicular to the pressing direction during vacuum hot pressing [63]. Increase in reinforcement

(graphene/MWCNTs) content leads to increase in surface agglomeration during milling rather than dispersion of reinforcement in the matrix [64]. The other possibility is the presence of reinforcement at grain boundary hinders the sintering, and as a result the porosity increases. The schematic of the process leading to formation of layered structure of AA2219-graphene and AA2219-MWCNT composite is shown in Fig. 9.

Hardness

The Brinell hardness of AA2219-graphene and AA2219-MWCNT composites is presented in Fig. 10a and b, respectively. The 6-h ball-milled sample shows a significant improvement in hardness compared to unreinforced AA2219. This may be mainly due to the grain refinement and strain hardening of powder particles during ball milling. Eldesouky et al. [65] observed an improvement in hardness with ball milling compared to unmilled sample. No further improvement in hardness was observed with addition of graphene/MWCNT to AA2219 matrix. In both systems (graphene/MWCNT), AA2219 reinforcement with 0.5 wt.% exhibited highest hardness value. Further addition of reinforcement reduced the hardness of composites. This is attributed to the clustering/agglomeration of nanoparticles and presence of porosities. The dark layer with network structure at grain boundaries increases with reinforcement (graphene/MWCNT) content and hinders the sintering process and results porosity. It is known that the presence of reinforcement clusters at grain boundaries inhibits the neck growth between matrix powder particles during sintering and results in insufficient densification and affects the properties of composite [49]. The other possibility is that the weak dark layer (reinforcement/porosity) at grain boundaries slides during Brinell hardness testing resulting in lower hardness values [63]. Bradbury et al. [46]

Fig. 8 Optical micrographs of the polished cross section of compacts fabricated by vacuum hot pressing (a) ARH, (b) AMH, (c) A0.5GH, (d) A1GH, (e) A2GH, (f) A0.5CH, (g) A1CH and (h) A2CH



obtained a maximum hardness for Al-MWCNT composites reinforced with 6 wt.%, and further addition did not result in any improvement in hardness. Bustamante et al. [28] observed an increase in hardness of Al-MWCNT composite with increasing reinforcement up to 1.75 wt.%

which subsequently decreased for 2 wt.% sample. In another study, Esawi et al. [66] observed a lower hardness value for Al-5 wt.% sample compared to Al-2 wt.% MWCNT sample. Tian et al. [67] fabricated AA7075-graphene composites at 50 MPa by using SPS and

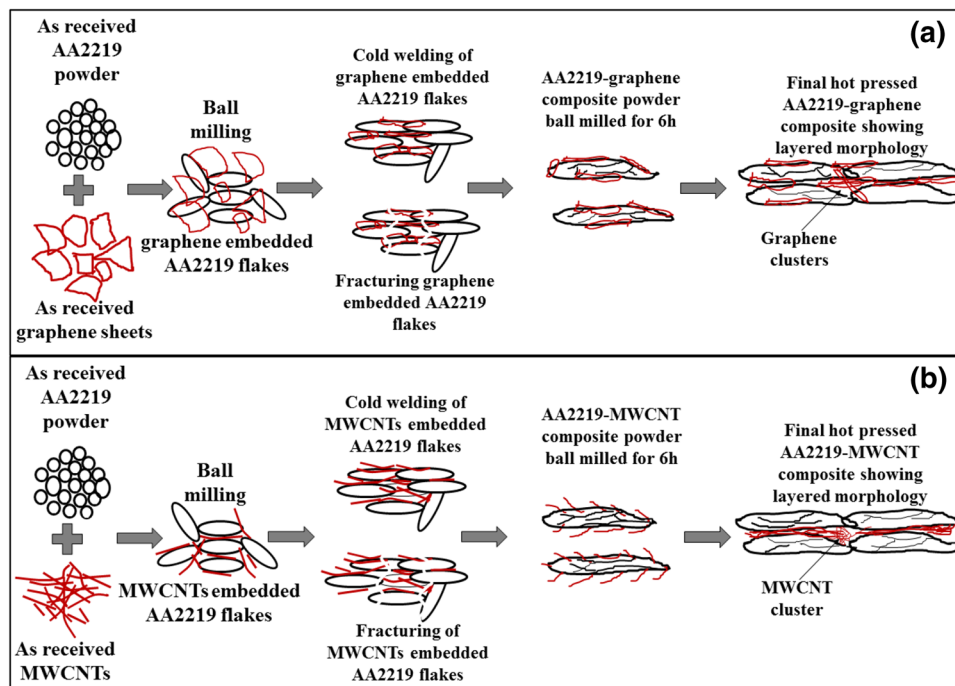


Fig. 9 Schematic of morphological changes occurring during fabrication of (a) AA2219-graphene and (b) AA2219-MWCNT composite powders by high-energy ball milling followed by vacuum hot pressing

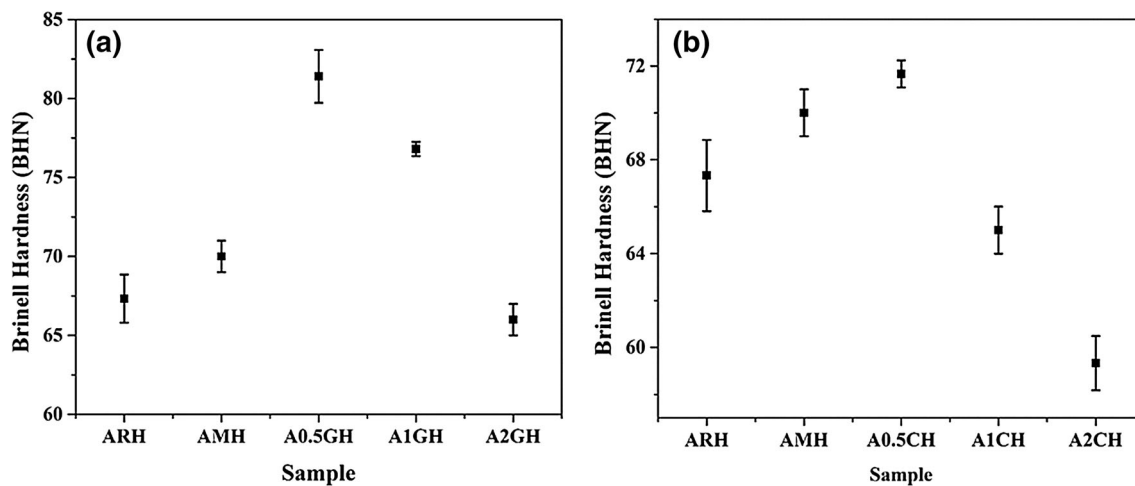


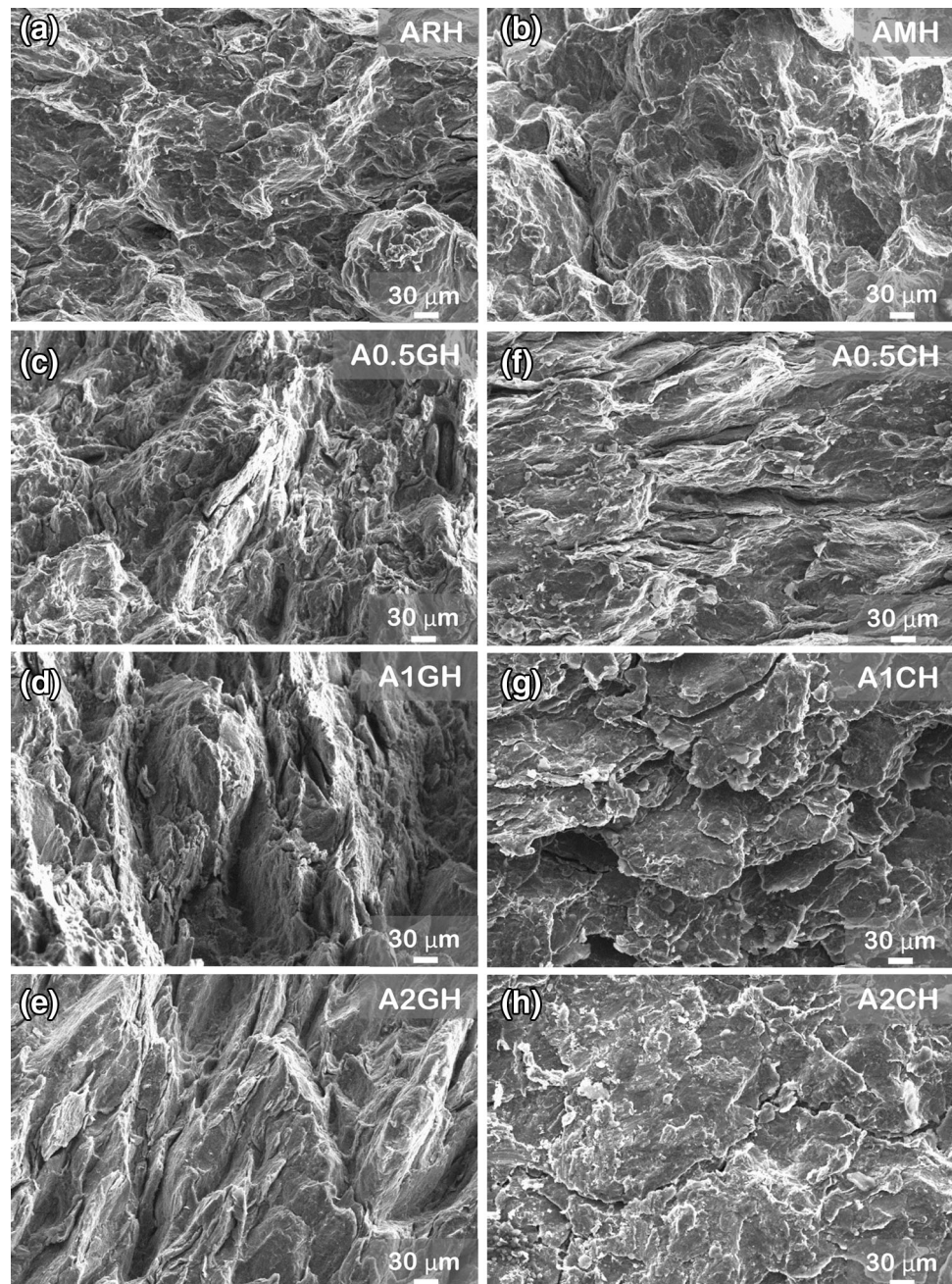
Fig. 10 Brinell hardness of the (a) AA2219-graphene and (b) AA2219-MWCNT composites fabricated by vacuum hot pressing

observed decrease in Vickers hardness above 1 wt.% graphene loading. It was also observed that the graphene-reinforced AA2219 composites exhibited higher hardness values compared to MWCNT-reinforced composites with same reinforcement content. This may be due to the morphological difference between graphene and MWCNT. The sheet morphology of graphene can cover AA2219 powder particles more effectively compared to tube-like MWCNTs and provide more matrix–reinforcement contact points which lead to better sintering [29].

Fracture Surface Analysis

Figure 11 compares the fracture surfaces of as-received AA2219 and 6-h ball-milled AA2219-graphene/MWCNT composites processed by vacuum hot pressing. Compared to the as-received AA2219 (Fig. 11a), the 6-h ball-milled AA2219 (Fig. 11b) showed a change in the morphology of fracture surface. The fully ductile morphology observed in the as-received AA2219 sample is absent in the fracture surface of 6-h milled AA2219 sample which

Fig. 11 SEM images of fracture surfaces: (a) ARH, (b) AMH, (c) A0.5GH, (d) A1GH, (e) A2GH, (f) A0.5CH, (g) A1CH and (h) A2CH



showed some flat regions, microcavities and voids. This indicates that the ductility of sample decreased with ball milling which may be attributed to the strain hardening due to ball milling. It can be seen that the ductile dimples diminished with addition of reinforcement (graphene/MWCNT) (Fig. 11c–h). The severity of layered morphology increases and the size of the dimples decreases significantly when graphene/MWCNT is added to the AA2219 matrix. The MWCNTs are embedded in the flaky-shaped AA2219 particles as observed in Fig. 11g. The size and number of microvoids/microcavities

increased with increasing reinforcement percentage. As discussed earlier, increase in reinforcement (graphene/MWCNTs) content leads to increase in surface agglomeration during milling rather than their dispersion into the matrix. The agglomerated/clustered regions of graphene/MWCNT at particle boundaries will be weaker regions, and the nucleation of crack occurs easily, and therefore, the subsequent propagation of crack occurs through particle boundaries as shown in Fig. 11h. The schematic representation of crack propagation through particle boundaries is presented in Fig. 12.

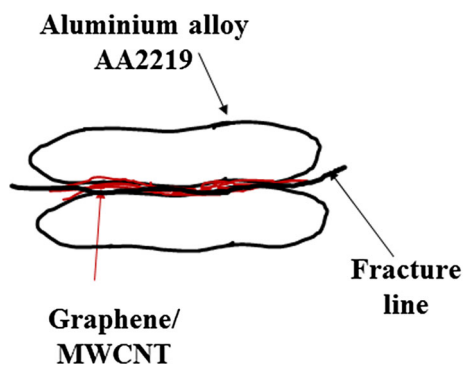


Fig. 12 Schematic of crack propagation along particle interfaces in AA2219-graphene/MWCNT composites

Conclusions

1. High-density AA2219-graphene/MWCNT nanocomposites have been successfully fabricated by high-energy ball milling followed by vacuum hot pressing.
2. The high-energy ball milling of composite powders up to 6 h resulted in a lamellar structure with graphene/MWCNT between particle boundaries.
3. DSC analysis shows that the detrimental aluminium carbide (Al_4C_3) is not formed while heating composite powders from room temperature to 650 °C as confirmed by XRD analysis.
4. The composite with 0.5 wt.% reinforcement (graphene/MWCNT) content exhibits the highest Brinell hardness. Further addition of graphene/MWCNT (1 and 2 wt.%) leads to decrease in hardness of the composites owing to the agglomeration of reinforcement at particle interfaces.
5. The ductility of composites decreased with addition of reinforcement (graphene/MWCNT), and it was confirmed by fracture analysis.
6. The present study reveals that graphene is a better reinforcement compared to MWCNTs in aluminium matrix.

Acknowledgments The authors wish to thank Director VSSC for giving permission to publish this work. This research was financially supported by the Indian Space Research Organization (ISRO/RES/3/630/12-13).

References

1. S.R. Bakshi, V. Singh, S. Seal, A. Agarwal, Aluminum composite reinforced with multiwalled carbon nanotubes from plasma spraying of spray dried powders. *Surf. Coat. Technol.* **203**, 1544–1554 (2009)
2. A. Dorri Moghadam, E. Omrani, P.L. Menezes, P.K. Rohatgi, Mechanical and tribological properties of self-lubricating metal matrix nanocomposites reinforced by carbon nanotubes (CNTs) and graphene—a review. *Compos. Part B Eng.* **77**, 402–420 (2015)
3. Z.M. Gasem, Fatigue crack growth behavior in powder-metalurgy 6061 aluminium alloy reinforced with submicron Al_2O_3 particulates. *Compos. Part B Eng.* **43**, 3020–3025 (2012)
4. L. Dyachkova, E.E. Feldshtein, On the properties of composites based on sintered bronze with alumina additives. *Compos. Part B Eng.* **45**, 239–247 (2013)
5. M. Bastwros, G.Y. Kim, C. Zhu, K. Zhang, S. Wang, X. Tang, X. Wang, Effect of ball milling on graphene reinforced Al6061 composite fabricated by semi-solid sintering. *Compos. Part B Eng.* **60**, 111–118 (2014)
6. M.O. Bodunrin, K.K. Alaneme, L.H. Chown, Aluminium matrix hybrid composites: a review of reinforcement philosophies; mechanical, corrosion and tribological characteristics. *J. Mater. Res. Technol.* **4**, 434–445 (2015)
7. S.K. Singhal, R. Pasricha, M. Jangra, R. Chahal, S. Teotia, R.B. Mathur, Carbon nanotubes: amino functionalization and its application in the fabrication of Al-matrix composites. *Powder Technol.* **215–216**, 254–263 (2012)
8. Z. Gnjidić, D. Božić, M. Mitkov, The influence of SiC particles on the compressive properties of metal matrix composites. *Mater. Charact.* **47**, 129–138 (2001)
9. V. Umasankar, S. Karthikeyan, M.A. Xavier, The influence of electroless nickel coated SiC on the interface strength and microhardness of aluminium composites. *J. Mater. Environ. Sci.* **5**, 153–158 (2014)
10. H. Hocheng, S.B. Yen, T. Ishihara, B.K. Yen, Fundamental turning characteristics of a tribology-favored graphite/aluminum alloy composite material. *Compos. Part A: Appl. Sci. Manuf.* **28**, 883–890 (1997)
11. A.R. Kennedy, S.M. Wyatt, Characterising particle–matrix interfacial bonding in particulate Al–TiC MMCs produced by different methods. *Compos. Part A: Appl. Sci. Manuf.* **32**, 555–559 (2001)
12. M. Kouzeli, A. Mortensen, Size dependent strengthening in particle reinforced aluminium. *Acta Mater.* **50**, 39–51 (2002)
13. K. Scida, P.W. Stege, G. Haby, G.A. Messina, C.D. García, Recent applications of carbon-based nanomaterials in analytical chemistry: critical review. *Anal. Chim. Acta* **691**, 6–17 (2011)
14. B.T. Zhang, X. Zheng, H.F. Li, J.M. Lin, Application of carbon-based nanomaterials in sample preparation: a review. *Anal. Chim. Acta* **784**, 1–17 (2013)
15. A.K. Geim, K.S. Novoselov, The rise of graphene. *Nat. Mater.* **6**, 183–191 (2007)
16. K.S. Novoselov, A.K. Geim, S.V. Morozov, D. Jiang, Y. Zhang, S.V. Dubonos, I.V. Grigorieva, A.A. Firsov, Electric field effect in atomically thin carbon films. *Science* **306**, 666–669 (2004)
17. J. Wang, Z. Li, G. Fan, H. Pan, Z. Chen, D. Zhang, Reinforcement with graphene nanosheets in aluminum matrix composites. *Scr. Mater.* **66**, 594–597 (2012)
18. M. Rashad, F. Pan, A. Tang, M. Asif, Effect of graphene nanoplatelets addition on mechanical properties of pure aluminum using a semi-powder method. *Prog. Nat. Sci. Mater. Int.* **24**, 101–108 (2014)
19. C. Lee, X. Wei, J.W. Kysar, J. Hone, Measurement of the elastic properties and intrinsic strength of monolayer graphene. *Science* **321**, 385–388 (2008)
20. A.A. Balandin, S. Ghosh, W. Bao, I. Calizo, D. Teweldebrhan, F. Miao, C.N. Lau, Superior thermal conductivity of single-layer graphene. *Nano Lett.* **8**, 902–907 (2008)
21. K.I. Bolotin, K.J. Sikes, Z. Jiang, M. Klima, G. Fudenberg, J. Hone, P. Kim, H.L. Stormer, Ultrahigh electron mobility in suspended graphene. *Solid State Commun.* **146**, 351–355 (2008)
22. S. Stankovich, D.A. Dikin, G.H.B. Dommett, K.M. Kohlhaas, E.J. Zimney, E.A. Stach, R.D. Piner, S.T. Nguyen, R.S. Ruoff,

- Graphene-based composite materials. *Nature* **442**, 282–286 (2006)
23. S. Iijima, Helical microtubules of graphitic carbon. *Nature* **354**, 56–58 (1991)
 24. M.M.J. Treacy, T.W. Ebbesen, J.M. Gibson, Exceptionally high Young's modulus observed for individual carbon nanotubes. *Nature* **381**, 678–680 (1996)
 25. R.S. Ruoff, D. Qian, W.K. Liu, Mechanical properties of carbon nanotubes: theoretical predictions and experimental measurements. *C. R. Phys.* **4**, 993–1008 (2003)
 26. C.M. Hussain, S. Mitra, Micropreconcentration units based on carbon nanotubes (CNT). *Anal. Bioanal. Chem.* **399**, 75–89 (2011)
 27. D. Chunfeng, Z. Xuexi, W. Dezun, Chemical stability of carbon nanotubes in the 2024 Al matrix. *Mater. Lett.* **61**, 904–907 (2007)
 28. R. Pérez-Bustamante, C.D. Gómez-Esparza, I. Estrada-Guel, M. Miki-Yoshida, L. Licea-Jiménez, S.A. Pérez-García, R. Martínez-Sánchez, Microstructural and mechanical characterization of Al-MWCNT composites produced by mechanical milling. *Mater. Sci. Eng. A* **502**, 159–163 (2009)
 29. S.E. Shin, H.J. Choi, J.H. Shin, D.H. Bae, Strengthening behavior of few-layered graphene/aluminum composites. *Carbon* **82**, 143–151 (2015)
 30. R. Pérez-Bustamante, F. Pérez-Bustamante, I. Estrada-Guel, L. Licea-Jiménez, M. Miki-Yoshida, R. Martínez-Sánchez, Effect of milling time and CNT concentration on hardness of CNT/Al 2024 composites produced by mechanical alloying. *Mater. Charact.* **75**, 13–19 (2013)
 31. Z.Y. Liu, S.J. Xu, B.L. Xiao, P. Xue, W.G. Wang, Z.Y. Ma, Effect of ball-milling time on mechanical properties of carbon nanotubes reinforced aluminum matrix composites. *Compos. Part A: Appl. Sci. Manuf.* **43**, 2161–2168 (2012)
 32. A. Esawi, K. Morsi, Dispersion of carbon nanotubes (CNTs) in aluminum powder. *Compos. Part A: Appl. Sci. Manuf.* **38**, 646–650 (2007)
 33. S.F. Bartolucci, J. Paras, M.A. Rafiee, J. Rafiee, S. Lee, D. Kapoor, N. Koratkar, Graphene-aluminum nanocomposites. *Mater. Sci. Eng. A* **528**, 7933–7937 (2011)
 34. J. Liu, U. Khan, J. Coleman, B. Fernandez, P. Rodriguez, S. Naher, D. Brabazon, Graphene oxide and graphene nanosheet reinforced aluminium matrix composites: powder synthesis and prepared composite characteristics. *Mater. Des.* **94**, 87–94 (2016)
 35. X. Gao, H. Yue, E. Guo, H. Zhang, X. Lin, L. Yao, B. Wang, Preparation and tensile properties of homogeneously dispersed graphene reinforced aluminum matrix composites. *Mater. Des.* **94**, 54–60 (2016)
 36. R. Pérez-Bustamante, D. Bolaños-Morales, J. Bonilla-Martínez, I. Estrada-Guel, R. Martínez-Sánchez, Microstructural and hardness behavior of graphene-nanoplatelets/aluminum composites synthesized by mechanical alloying. *J. Alloys Compd.* **615**, S578–S582 (2014)
 37. S. Nasimul, L. Kumar, Mechanical properties of aluminium based metal matrix composites reinforced with graphite nanoplatelets. *Mater. Sci. Eng. A* **667**, 16–32 (2016)
 38. J.L. Li, Y.C. Xiong, X.D. Wang, S.J. Yan, C. Yang, W.W. He, J.Z. Chen, S.Q. Wang, X.Y. Zhang, S.L. Dai, Microstructure and tensile properties of bulk nanostructured aluminum/graphene composites prepared via cryomilling. *Mater. Sci. Eng. A* **626**, 400–405 (2015)
 39. H. Zhang, C. Xu, W. Xiao, K. Ameyama, C. Ma, Enhanced mechanical properties of Al5083 alloy with graphene nanoplates prepared by ball milling and hot extrusion. *Mater. Sci. Eng., A* **658**, 8–15 (2016)
 40. H. Kwon, J. Mondal, K.A. AlOgab, V. Sammelselg, M. Takamichi, A. Kawaski, M. Leparoux, Graphene oxide-reinforced aluminum alloy matrix composite materials fabricated by powder metallurgy. *J. Alloys Compd.* **698**, 807–813 (2017)
 41. J.Z. Liao, M.J. Tan, I. Sridhar, Spark plasma sintered multi-wall carbon nanotube reinforced aluminum matrix composites. *Mater. Des.* **31**, S96–S100 (2010)
 42. R. Pérez-Bustamante, I. Estrada-Guel, W. Antúnez-Flores, M. Miki-Yoshida, P.J. Ferreira, R. Martínez-Sánchez, Novel Al-matrix nanocomposites reinforced with multi-walled carbon nanotubes. *J. Alloys Compd.* **450**, 323–326 (2008)
 43. I.Y. Kim, J.H. Lee, G.S. Lee, S.H. Baik, Y.J. Kim, Y.Z. Lee, Friction and wear characteristics of the carbon nanotube-aluminum composites with different manufacturing conditions. *Wear* **267**, 593–598 (2009)
 44. K. Morsi, A.M.K. Esawi, S. Lanka, A. Sayed, M. Taher, Spark plasma extrusion (SPE) of ball-milled aluminum and carbon nanotube reinforced aluminum composite powders. *Compos. Part A: Appl. Sci. Manuf.* **41**, 322–326 (2010)
 45. M. Majid, G.H. Majzoubi, G.A. Noozad, A. Reihani, S.Z. Mortazavi, M.S. Gorji, Fabrication and mechanical properties of MWCNTs-reinforced aluminum composites by hot extrusion. *Rare Met.* **31**, 372–378 (2012)
 46. C.R. Bradbury, J.K. Gomon, L. Kollo, H. Kwon, M. Leparoux, Hardness of multi wall carbon nanotubes reinforced aluminium matrix composites. *J. Alloys Compd.* **585**, 362–367 (2014)
 47. T. He, X. He, P. Tang, D. Chu, X. Wang, P. Li, The use of cryogenic milling to prepare high performance Al2009 matrix composites with dispersive carbon nanotubes. *Mater. Des.* **114**, 373–382 (2017)
 48. C. Deng, X. Zhang, D. Wang, Q. Lin, A. Li, Preparation and characterization of carbon nanotubes/aluminum matrix composites. *Mater. Lett.* **61**, 1725–1728 (2007)
 49. N. Saheb, Sintering behavior of CNT reinforced Al6061 and Al2124 nanocomposites. *Adv. Mater. Sci. Eng.* **2014**, 9 (2014)
 50. L. Wang, H. Choi, J.M. Myoung, W. Lee, Mechanical alloying of multi-walled carbon nanotubes and aluminium powders for the preparation of carbon/metal composites. *Carbon* **47**, 3427–3433 (2009)
 51. K. Morsi, A. Esawi, Effect of mechanical alloying time and carbon nanotube (CNT) content on the evolution of aluminum (Al)-CNT composite powders. *J. Mater. Sci.* **42**, 4954–4959 (2007)
 52. Y. Wu, G.Y. Kim, A.M. Russell, Effects of mechanical alloying on an Al6061-CNT composite fabricated by semi-solid powder processing. *Mater. Sci. Eng. A* **538**, 164–172 (2012)
 53. A.M. Samuel, J. Gauthier, F.H. Samuel, Microstructural aspects of the dissolution and melting of Al₂Cu phase in Al–Si alloys during solution heat treatment. *Metall. Mater. Trans. A* **27A**, 1785–1798 (1996)
 54. C.F. Deng, D.Z. Wang, X.X. Zhang, A.B. Li, Processing and properties of carbon nanotubes reinforced aluminum composites. *Mater. Sci. Eng. A* **444**, 138–145 (2007)
 55. N. Nayan, S.V.S.N. Murty, S.C. Sharma, K.S. Kumar, P.P. Sinha, Calorimetric study on mechanically milled aluminum and multi-wall carbon nanotube composites. *Mater. Charact.* **62**, 1087–1093 (2011)
 56. A.M.K. Esawi, K. Morsi, A. Sayed, M. Taher, S. Lanka, The influence of carbon nanotube (CNT) morphology and diameter on the processing and properties of CNT-reinforced aluminium composites. *Compos. Part A: Appl. Sci. Manuf.* **42**, 234–243 (2011)
 57. L. Bokobza, J.-L. Bruneel, M. Couzi, Raman spectra of carbon-based materials (from graphite to carbon black) and of some silicone composites. *Carbon* **1**, 77–94 (2015)
 58. X. Zhu, Y.G. Zhao, M. Wu, H.Y. Wang, Q.C. Jiang, Effect of initial aluminum alloy particle size on the damage of carbon nanotubes during ball milling. *Materials* **9**, 173 (2016)

59. L. Kumar, S. Nasimul Alam, S.K. Sahoo, Mechanical properties, wear behavior and crystallographic texture of Al-multiwalled carbon nanotube composites developed by powder metallurgy route. *J. Compos. Mater.* **51**, 1099–1117 (2016)
60. T. Peng, I. Chang, Uniformly dispersion of carbon nanotube in aluminum powders by wet shake-mixing approach. *Powder Technol.* **284**, 32–39 (2015)
61. P. Van Trinh, N. Van Luan, P.N. Minh, D.D. Phuong, Effect of sintering temperature on properties of CNT/Al composite prepared by capsule-free hot isostatic pressing technique. *Trans. Indian Inst. Met.* **70**, 947–955 (2017)
62. A.M.K. Esawi, M.A. El Borady, Carbon nanotube-reinforced aluminium strips. *Compos. Sci. Technol.* **68**, 486–492 (2008)
63. A.K. Shukla, N. Nayan, S.V.S.N. Murty, S.C. Sharma, P. Chandran, S.R. Bakshi, K.M. George, Processing of copper-carbon nanotube composites by vacuum hot pressing technique. *Mater. Sci. Eng. A* **560**, 365–371 (2013)
64. N. Nayan, A.K. Shukla, P. Chandran, S.R. Bakshi, S.V.S.N. Murty, B. Pant, P.V. Venkitakrishnan, Processing and characterization of spark plasma sintered copper/carbon nanotube composites. *Mater. Sci. Eng. A* **682**, 229–237 (2017)
65. A. Eldesouky, M. Johnsson, H. Svengren, M.M. Attallah, H.G. Salem, Effect of grain size reduction of AA2124 aluminum alloy powder compacted by spark plasma sintering. *J. Alloys Compd.* **609**, 215–221 (2014)
66. A.M.K. Esawi, K. Morsi, A. Sayed, M. Taher, S. Lanka, Effect of carbon nanotube (CNT) content on the mechanical properties of CNT-reinforced aluminium composites. *Compos. Sci. Technol.* **70**, 2237–2241 (2010)
67. W. Tian, S. Li, B. Wang, X. Chen, J. Liu, M. Yu, Graphene-reinforced aluminum matrix composites prepared by spark plasma sintering. *Int. J. Min. Metall. Mater.* **23**, 723–729 (2016)